

# Riversand: a new tool for efficient computation of catchmentwide erosion rates

Konstanze Stübner<sup>1,\*</sup>, Greg Balco<sup>2</sup>, Nils Schmeisser<sup>1</sup>

<sup>1</sup> Institute of Ion Beam Physics and Materials Research, Helmholtz-Zentrum Dresden-Rossendorf, 01328 Dresden, Germany

<sup>2</sup> Berkeley Geochronology Center, Berkeley, CA 94709, USA

\* k.stuebner@hzdr.de

## Abstract

In situ cosmogenic  $^{10}\text{Be}$  (and  $^{26}\text{Al}$ ) concentrations in alluvial sediments provide a spatially averaged signal of the erosion rate of the catchment area. Catchmentwide erosion rates reflect the production rate of the entire basin, and their calculation requires knowledge of the complete production rate model. Available calculators determine production rates on a pixel-based approach and achieve computational efficiency by relying on a scaling method that ignores geomagnetic field strength variations. Here we introduce a new python-based tool that determines erosion rates based on the hypsometry of the catchment. The method relies on the fact that production rates are much more sensitive to changes in elevation than latitude. Our tool has two main advantages: (1) Computation time is short (<30 seconds) and independent of the scaling method; there is no need to neglect magnetic field variations. (2) Because production rate scaling is performed by a widely-used online calculator (<http://stoneage.ice-d.org> or <http://stoneage.hzdr.de>), the results are fully comparable to exposure ages or point-based erosion rates determined with the same calculator; future updates to production rate scaling are immediately effective for catchmentwide erosion rate calculation. We demonstrate in two case studies that: (1) For similar scaling methods, our calculator reproduces pixel-based results within a few percent. (2) Erosion rates determined with different scaling methods may differ by >20 %, differences can vary systematically with erosion rate, and using a time-constant scaling method may result in a bias in the interpretation of catchmentwide erosion rates.

## 1. Introduction

Cosmogenic radionuclide inventories in fluvial and alluvial sediments reflect the sediment flux out of the catchment area and have been used to estimate basin-average erosion rates for more than 25 years (Brown et al. 1995; Bierman and Steig 1996; Granger et al. 1996; Portenga and Bierman 2011). Calculating an erosion rate or an exposure age requires the cosmogenic radionuclide production rate, which is specific to the site (latitude, longitude and elevation above sea level). Near the Earth's surface, production of in situ cosmogenic  $^{10}\text{Be}$  and  $^{26}\text{Al}$  is dominated by high-energy spallation; at depth production by negative muon capture and fast muon interaction becomes significant. Site-specific production rates are calculated using one of several published scaling methods (Lal 1991; Stone 2000; Dunai 2001; Lifton et al. 2008; Desilets et al. 2006; Lifton et al. 2014) and a sea-level and high-latitude reference production rate (e.g. Borchers et al. 2016; Martin et al. 2017). The calculation of a site-specific production rate also depends on the choice of an atmospheric model to convert elevation to atmospheric depth, a palaeomagnetic framework to account for the effects of the Earth's magnetic field on the cosmic-ray flux, the attenuation length in rock and the choice of a model of muogenic nuclide production. Online calculators (Balco et al. 2008; Marrero et al. 2015; Martin et al. 2017) harmonise these calculations and have greatly improved the reproducibility of cosmogenic nuclide exposure ages and erosion rates.

Cosmogenic nuclide concentrations in river sediments provide a spatially averaged signal of the rates at which the catchment is eroding and can be used to quantify erosion processes within landscapes (Bierman and Steig 1996). The calculation of catchment-averaged erosion rates assumes that erosion rates are constant, that the catchment area is in isotopic steady state, and that the sediment is well mixed and sediment storage within the basin is negligible (e.g. von Blanckenburg 2005). Because production rates are site specific, the calculation of catchmentwide erosion rates depends on the complete production rate model of the basin. For settings with little variability in production rates a single "basin-wide" production rate determined from the basin mean latitude, longitude and elevation may yield a good approximation of the catchmentwide erosion rate (Brown et al. 1995). More advanced approaches are based on spatially resolved production rates determined from a pixel array that represents the catchment topography (e.g. Belmont et al. 2007; Portenga and Biermann 2011; Lupker et al. 2012; Godard et al. 2014; Scherler et al. 2014). For computational efficiency these calculations are often based on the time-constant production rate scaling of Lal (1991)/Stone (2000), which does not take into account the Earth's magnetic field variations, although solutions that incorporate a geomagnetic correction after Nishiizumi et al. (1989) have been developed (Scherler et al. 2014; Charreau et al 2019).

Previously published algorithms to calculate catchmentwide erosion rates (Mudd et al. 2016; Charreau et al. 2019) are independent from existing online calculators (Balco et al. 2008; Marrero et al. 2015; Martin et al. 2017), even if the calculations are based on the same scaling methods that are implemented in the online calculators. Catchmentwide erosion rates determined in this way are therefore not fully comparable to exposure ages and point-based erosion rates calculated with the existing calculators although the discrepancies may, in practice, be small compared to the uncertainties arising from the assumptions that are made when a basin-average erosion rate is determined from a river sediment sample (e.g. von Blanckenburg 2005). We introduce 'riversand', a new python package for the efficient computation of catchmentwide erosion rates fully integrated with the existing online exposure age and erosion rate calculator provided and maintained by G. Balco (Balco et al. 2008), (<http://hess.ess.washington.edu>, <http://stoneage.ice-d.org>, or <http://stoneage.hzdr.de>). The package is published in the Python Package Index repository (<https://pypi.org/project/riversand/>) and includes an installation guide and example scripts. It is a key feature of riversand that all future updates to the production rate calculation of the online calculator are immediately effective for the calculation of catchmentwide erosion rates and that the results are therefore fully comparable and future-proof. This contribution provides a description of the riversand calculator and an illustrative comparison to erosion rates calculated with the Basinga cell-by-cell GIS toolbox (Charreau et al. 2019) and the CAIRN method (Mudd et al. 2016).

## 2. Principles

Every location within a catchment has its unique (time-dependent) production rate, which for a given erosion rate can be expressed as a function of the geographic coordinates (latitude and longitude) and the elevation above sea level. Note that we use the term "erosion" instead of "denudation" to refer to the removal of mass from the Earth's surface without the distinction between physical erosion and chemical weathering to keep in line with the usage of "erosion" in the online calculator. In practice, production rates are much more sensitive to changes in elevation than latitude (Lal 1991). Following the approach of Bierman and Steig (1996), we use the catchment hypsometry to subdivide the catchment into regions of similar elevation with a representative nuclide production rate  $P_i$  for each subregion  $i$  (Fig. 1a, b).

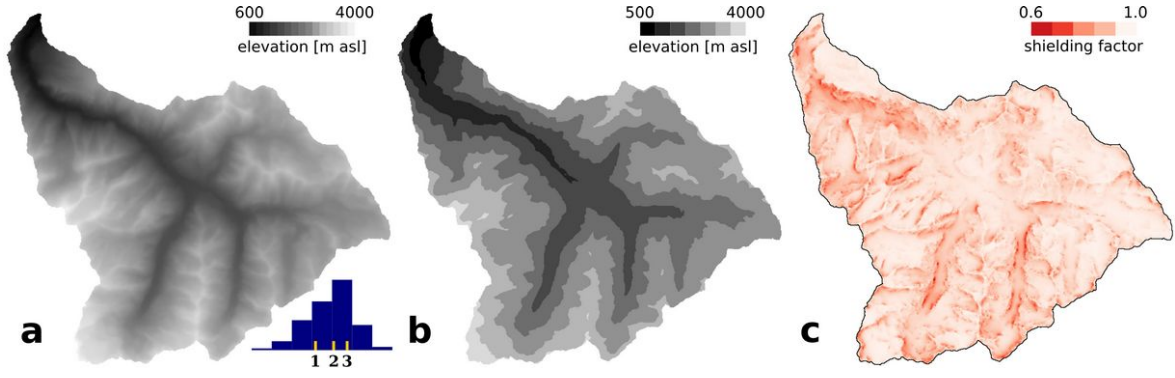


**Figure 1:** Example catchment, area 257 km<sup>2</sup>, elevations 640 to 4020 m asl. (a) Topography from a NASADEM digital elevation model, projected to UTM 32N, pixel resolution 35 m (NASA JPL 2021). Inset shows a histogram of elevations with a bin size of 500 m; quartiles (1: 2082, 2: 2532, 3: 2850 m asl) are indicated. (b) Catchment topography binned with a bin size of 500 m, i.e. subdivided into seven subregions. (c) Topographic shielding raster dataset calculated from the same elevation model using the toposhielding function of TopoToolbox (Schwanghart and Scherler 2014).

For time-constant production rates after Lal/Stone the production rate of the entire catchment may be calculated as an area-weighted average of the production rates of the subregions. For the more general case of a time-dependent production rate model the cosmogenic nuclide production of each subregion  $N_{\text{pred},i}(E)$  is calculated by the online calculator for a given erosion rate  $E$  based on the mean elevation of the subregion  $i$  and the centroid coordinates of the entire catchment (Fig. 2, 3). The calculation of  $N_{\text{pred},i}(E)$  by the online calculator is described in Balco et al. (2008; their Eq. 2). Shielding factors (e.g., topographic shielding, snow shielding, or vegetation shielding) may be assumed constant for the entire catchment. Alternatively, if spatially resolved shielding factors are available a mean shielding factor is determined for each subregion  $i$  of the elevation-binned catchment and included in the calculation of  $N_{\text{pred},i}(E)$  (Fig. 1c). The predicted nuclide concentration at the catchment outlet for the given erosion rate  $E$  is the sum of predicted nuclide concentrations of each subregion  $N_{\text{pred},i}(E)$  normalized by the area of the subregion  $A_i$ :

$$N_{\text{pred}}(E) = \frac{1}{A} \cdot \sum_{i=1}^n A_i \cdot N_{\text{pred},i}(E) \quad (1)$$

To calculate the catchmentwide erosion rate  $E$  that corresponds to the measured nuclide concentration at the catchment outlet  $N_{\text{meas}}$  we use the online calculator to predict nuclide concentrations for a suite of different erosion rates  $E_n$  and fit a polynomial function of the form  $y = a/x^2 + b/x + c$  to these data (Fig. 4). The uncertainty in  $E$ ,  $\text{del}E$ , is determined from the uncertainty in the measured nuclide concentration,  $\text{del}N_{\text{meas}}$ , and the empirical polynomial function; it does not include the uncertainties in the production rate estimates.  $\text{del}E$  is asymmetric and generally smaller for high nuclide concentrations or low erosion rates.

Although the catchmentwide erosion rate  $E$  may be determined iteratively from an arbitrary set of initial erosion rates  $E_n$ , an efficient computation of  $E$  is achieved with a suitable set of initial values. We estimate the bracket of initial erosion rates,  $E_{\text{min}}$  and  $E_{\text{max}}$ , from the first and third quartile of the catchment hypsometry (Fig. 1a, inset); the computation of  $E_{\text{min}}$  and  $E_{\text{max}}$  is performed by the online calculator. By default the initial erosion rates are six values that are logarithmically distributed from  $E_{\text{min}}$  to  $E_{\text{max}}$  (Fig. 4).

	bins	elevation	shielding	area	lat	long	wt
0	(500, 1000)	877.0	0.905759	2.6	45.6	7.348	0.01017
1	(1000, 1500)	1306.0	0.887406	12.3	45.6	7.348	0.04787
2	(1500, 2000)	1771.0	0.914313	41.3	45.6	7.348	0.16021
3	(2000, 2500)	2279.0	0.923123	66.7	45.6	7.348	0.25906
4	(2500, 3000)	2742.0	0.932478	95.8	45.6	7.348	0.37179
5	(3000, 3500)	3188.0	0.921473	34.5	45.6	7.348	0.13397
6	(3500, 4000)	3606.0	0.923750	4.3	45.6	7.348	0.01688
7	(4000, 4500)	4009.0	0.956851	0.0	45.6	7.348	0.00004

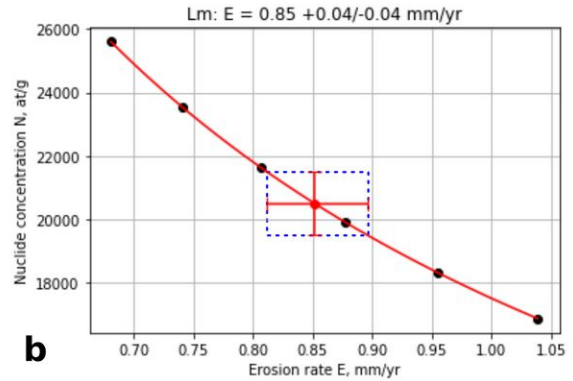
**Figure 2:** Table of the "hypsometry statistics" needed for the prediction of nuclide productions derived from the elevation-binned catchment (bin size 500 m): '*elevation*' and '*area*' are the mean elevation and the area in km<sup>2</sup> of each subregion, '*wt*' is the nomalised area. '*lat*' and '*long*' are the centroid coordinates of the catchment. In this example a mean shielding factor '*shielding*' was calculated for each subregion *i* from a topographic shielding raster (Fig. 1c).

	E_cmyr	NpredSt	NpredLm	NpredLSDn	St	Lm	LSDn
0	0.09	6143	6295	6237	62.5	64.0	63.5
1	0.09	8141	8352	8417	389.8	399.9	403.0
2	0.09	11483	11796	12132	1839.7	1889.8	1943.6
3	0.09	16172	16631	17534	4189.5	4308.5	4542.4
4	0.09	21778	22414	24243	8096.9	8333.4	9013.4
5	0.09	28010	28845	32045	3752.5	3864.4	4293.1
6	0.09	35439	36515	41655	598.3	616.5	703.2
7	0.09	45341	46737	54731	1.7	1.8	2.1

**Figure 3:** Table of predicted nuclide concentrations '*NpredSt*', '*NpredLm*', '*NpredLSDn*' for each subregion of the catchment determined from the hypsometry statistics (Fig. 2) for an erosion rate of 0.09 cm/yr for the three scaling methods currently implemented in the online calculator (St: time-independent Lal 1991/Stone 2000; Lm: time-dependent version of St; LSDn: time-dependent after Lifton et al. 2014). '*St*', '*Lm*', '*LSDn*' are the predicted nuclide concentrations normalized by the area of each subregion ('*wt*' in Fig. 2).

	St	Lm	LSDn
erosion_rate_cm_yr			
0.06807	24956.4	25607.4	27514.6
0.07409	22911.2	23527.1	25298.1
0.08063	21051.1	21635.1	23276.2
0.08776	19360.3	19914.2	21432.1
0.09551	17800.8	18328.4	19728.6
0.10390	16361.3	16864.1	18153.6

**a**



**b**

**Figure 4:** (a) Predicted nuclide concentrations at the catchment outlet for three different scaling methods '*St*', '*Lm*', '*LSDn*' and for six different erosion rates. (b) Predicted nuclide concentrations as a function of erosion rate for '*Lm*' scaling. The catchmentwide erosion rate  $E$  corresponding to the measured nuclide concentration at the catchment outlet,  $N_{\text{meas}}$ , is determined from the polynomial function  $y = a/x^2 + b/x + c$  fit to the data points (red line and point). The uncertainty in  $E$ ,  $delE$ , is determined from the uncertainty in the measured nuclide concentration,  $delN_{\text{meas}}$ , and the empirical polynomial function (red error bars and dashed line).

The scaling methods available in the riversand calculator are those that are implemented in the online calculator and described in Balco et al. (2008) and the online documentation at <http://stoneage.ice-d.org/>; currently these are 'St': a time-constant scaling method after Lal (1991) and Stone (2000); 'Lm': a time-dependent version of the Lal/Stone method that incorporates magnetic field fluctuations and solar modulation after Nishiizumi et al. (1989); and 'LSDn': a time-dependent and nuclide-specific scaling method after Lifton et al. (2014), which is also favoured by the CRONUScalc online calculator (Marrero et al. 2016). Geomagnetic corrections for Lm and



LSDn scaling are based on a composite geocentric/axial dipole field reconstruction (DGRF / SHA.DIF14k / GLOPAD models; [Lifton 2016](#)). Atmospheric scaling is based on the ERA-40 reanalysis ([Uppala et al. 2005](#)); the Stone/Radok atmospheric model ([Radok et al. 1996](#); [Stone 2000](#)) is also implemented and is recommended for sites in Antarctica. Muogenic production is approximated by a single erosion-rate dependent exponential ([Balco et al. 2008](#); [Balco 2017](#)). Reference production rates are sourced from the CRONUS-Earth primary data set (<http://calibration.ice-d.org/> accessed 2016-12-04).

Input data for the riversand calculator are: (1) a digital elevation model of the study area in an equal-area projection in geotiff format ("elevation raster"; for example [NASA JPL \(2021\)](#) NASADEM); (2) the catchment outline(s) as polygon shapefile; (3) a spreadsheet with sample and nuclide data corresponding to the input of the online calculator. In addition, there are two optional input datasets: (1) Shielding data may be provided as a constant value for each catchment or as a shielding raster dataset; for example, topographic shielding may be calculated from the elevation raster using the toposhielding function of the TopoToolbox ([Schwanghart and Scherler 2014](#)) and included in the calculation. (2) A raster dataset that classifies the catchment into "quartz-bearing" and "quartz-free" lithologies may be used to exclude the quartz-free portions of the catchment from the calculation ([Delunel et al. 2010](#)). The calculator has options to process a single catchment or multiple catchments. The workflow to using the riversand calculator comprises two steps: (1) Import and validate all input data. (2) Process the catchments by calling a single function that performs the calculations outlined above with specified parameters such as bin size for the catchment hypsometry and scaling method. The output includes catchmentwide erosion rates calculated with the available scaling methods (St, Lm, LSDn) as well as some catchment statistics (e.g. catchment area and mean elevation) and can be saved as a csv-file or an Excel spreadsheet. The calculator also saves images of the clipped catchments, the elevation histograms and the empirical function  $N_{\text{pred}}(E)$  (see Fig. 4b).

The riversand calculator communicates with the online calculator via a URL request. The performance depends on the number of values  $N_{\text{pred}}$  that need to be calculated by the online calculator. In particular, the computation will become slow or may fail if a very small elevation bin size is selected, i.e. if the table of hypsometry statistics (see Fig. 2) becomes very large. We recommend a bin size of 100 m for standard applications. On the other hand, the size or resolution of the catchment elevation model has little impact on computation times, and there is no need to resample the elevation model of a large catchment to a low resolution. The computation time for a single catchment is typically <30 seconds independent of the (time-constant or time-dependent) scaling method.

### 3. Examples

To illustrate the use of the riversand calculator we recalculated catchmentwide erosion rates published in two recent studies from the Western Alps ([Serra et al. 2022](#)) and the Peruvian Andes ([Reber et al. 2017](#)), respectively. Both study areas are from high-relief terrain where the effects of catchment hypsometry on production rates are expected to be most pronounced. Catchment sizes are 50-3300 km<sup>2</sup> (Western Alps) and 600-17000 km<sup>2</sup> (Peruvian Andes). Published erosion rates are 300 to 1500 mm/kyr in the Western Alps ([Serra et al. 2022](#); calculated with Basinga, [Charreau et al. 2019](#)) and 9 to 240 mm/kyr in the Peruvian Andes ([Reber et al. 2017](#); calculated with CAIRN, [Mudd et al. 2016](#)).

#### 3.1 High-relief catchments in the Western Alps

[Serra et al. \(2022\)](#) present <sup>10</sup>Be concentrations from 19 fluvial sediment samples in the Dora Baltea catchment in the Western Alps. Catchments are located 6.8 to 8.0°E and 45.4 to 46.0°N; catchment

areas range from 54 to 3320 km<sup>2</sup> with topographic relief 2400 to 4500 m and catchment mean elevation 2000 to 2500 m asl. The terrain is partly glaciated, and steep headwalls and deeply incised valleys cause significant topographic shielding. Reported <sup>10</sup>Be concentrations range from 1.08×10<sup>4</sup> to 4.85×10<sup>4</sup> atoms/grams quartz with analytical uncertainties typically 3 to 9 % (Serra et al. 2022). Catchmentwide erosion rates were calculated with Basinga (Charreau et al. 2019) using the Lal/Stone production rate scaling method (Lal 1991; Stone 2000) combined with the ERA-40 reanalysis database (Uppala et al. 2005) and the VDM database (Muscheler et al. 2005) for atmospheric and geomagnetic correction, respectively. Sea-level high-latitude reference production rate is 4.18±0.26 at/g/yr with a relative contribution of fast and negative muons of 0.27 % and 0.87 %, respectively (Charreau et al. 2019 after Braucher et al. 2011 and Martin et al. 2017). Erosion rates are corrected for topographic shielding using the toposhielding function of TopoToolbox (Schwanghart and Scherler 2014).

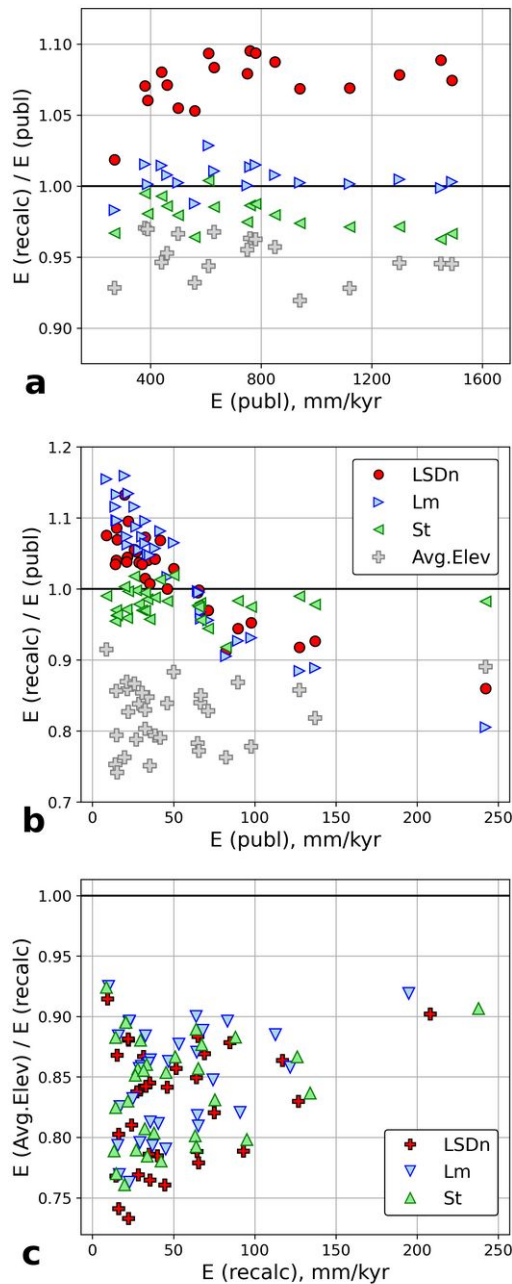


**Figure 5:** (a) Ratio of recalculated to published erosion rates for the Dora Baltea catchment, Western Alps (Serra et al. 2022) for St: Lal/Stone, Lm: modified Lal/Stone, LSDn: Lifton/Seto/Dunai scaling (see (b) for legend). Grey crosses show erosion rates calculated from the catchment mean elevation instead of the catchment hypsometry (Lm scaling). The Lm scaling (blue ► triangles) corresponds approximately to the modified Lal/Stone scaling method used in the original publication. (b) Same as (a) for the Peruvian Andes (Reber et al. 2017). Catchment mean-elevation erosion rates (grey crosses) are based on St scaling. The St scaling (green ◄ triangles) corresponds approximately to the Lal/Stone scaling method used in the original publication. (c) Ratio of erosion rates approximated from the catchment mean elevation ( $E(\text{Avg.Elev})$ ) to the results of the complete production model ( $E(\text{recalc})$ ) for the data set of Reber et al. (2017).

We compare the published results to erosion rates recalculated with the riversand calculator using the Lal/Stone (St), the modified time-dependent Lal/Stone (Lm) and the Lifton/Sato/Dunai (LSDn) scaling methods of the online calculator v.3 (Fig. 5a). The most notable differences of the Lm scaling compared to the Lal/Stone scaling used in [Serra et al. \(2022\)](#) are: (1) a different framework for geomagnetic corrections; (2) a different  $^{10}\text{Be}$  reference spallation production (riversand:  $4.208 \pm 0.316$  at/g/yr vs. Basinga:  $4.18 \pm 0.26$  at/g/yr); (3) a different muogenic production model. Both calculations use an attenuation length of spallation production of  $160 \text{ g/cm}^2$  and a rock density of  $2.7 \text{ g/cm}^3$ . The riversand recalculation is based on the NASADEM digital elevation model ([NASA JPL 2021](#)) resampled to a resolution of 35 m and an elevation histogram with a bin size of 100 m.

The differences between recalculated Lm erosion rates and the published values are mostly  $<2\%$  (Fig. 5a); this is within the rounding error, as the values are published to two significant figures. LSDn scaling yields 5-10 % higher values consistent with the results of a sensitivity analysis for similar latitudes and elevations by [Charreau et al. \(2019\)](#); their Figure 1), even though these authors ascertain that for many natural cases the difference between Lal/Stone and Lifton/Sato/Dunai scaling is small. St scaling yields values  $\leq 4\%$  lower than the published rates. The uncertainties on the erosion rates include the analytical uncertainties in measured  $^{10}\text{Be}$  concentrations and production rate uncertainties ([Charreau et al. 2019](#)) and the function  $N_{\text{pred}}(E)$  (this study), respectively; predicted uncertainties are similar for the published and the recalculated values (Supplementary Table S1).

In low-relief terrain with only minor variation in production rates, catchmentwide erosion rates may be approximated using a single production rate calculated from the mean elevation of the catchment ([Brown et al. 1995](#); [Blanckenburg 2005](#)). Figure 5a also shows erosion rates calculated from the centroid coordinates, mean elevation and mean topographic shielding of each catchment (Lm scaling). Because production varies approximately exponentially with elevation this approach generally underestimates the true erosion rates. In the present example, the results of this approach are  $\sim 2\text{-}8\%$  lower than values calculated from a complete production rate model of the catchment.

## 4.2 Large catchments in the Peruvian Andes

[Reber et al. \(2017\)](#) report  $^{10}\text{Be}$  concentrations from 42 fluvial sediment samples along the Pacific coast between  $6^\circ\text{S}$  and  $20^\circ\text{S}$  latitude. Catchment areas are  $>700 \text{ km}^2$  with several catchments  $>10000 \text{ km}^2$ . Peak elevations are  $>6000 \text{ m asl}$ . Reported  $^{10}\text{Be}$  concentrations range from  $8.5 \times 10^4$  to  $1.0 \times 10^6$  atoms/grams quartz with analytical uncertainties  $\sim 3\%$  ([Reber et al. 2017](#)). Catchmentwide erosion rates were calculated with CAIRN ([Mudd et al. 2016](#)) with the default parameters of the program and a rock density of  $2.65 \text{ g/cm}^3$ . CAIRN uses the time-constant Lal/Stone scaling method and the NCEP2 climate reanalysis data ([Compo et al. 2011](#)) for atmospheric scaling. The sea-level high-latitude reference production rate is  $4.30 \pm 0.39$  at/g/yr. Muogenic production is modelled as the sum of two exponential functions for fast and negative muons, respectively. Similar to Basinga ([Charreau et al. 2019](#)) and the current version of the online calculator, the spallation attenuation length is  $160 \text{ g/cm}^2$ . Topographic shielding is calculated as part of the CAIRN algorithm and follows the method of [Codilean \(2006\)](#).

Because of the large size of the study area and the large catchment areas [Reber et al. \(2017\)](#) use a 200-m resolution digital elevation model for the pixel-based calculation of catchmentwide erosion rates (resampled from a 90-m resolution SRTM digital elevation model, [Jarvis et al. 2008](#)). We recalculated erosion rates using a 100-m resolution NASADEM ([NASA JPL 2021](#)) and elevation histograms with a bin size of 100 m. Figure 5b compares recalculated rates (St, Lm and LSDn scaling) to published values. The St results are similar to ( $\sim 0\text{-}5\%$  lower than) published rates. Although [Mudd et al. \(2016\)](#) ascertain that the time-constant Lal/Stone scaling method

performs similar to the more recent Lifton/Sato/Dunai methods our recalculation shows that Lm and LSDn results differ up to 20 % and 10 % from published (Lal/Stone scaling) values, respectively (Fig. 5b). The ratios of recalculated LSDn to published Lal/Stone values vary systematically with erosion rate and are weakly to moderately correlated with catchment area ( $r = -0.57$ ), catchment mean elevation ( $r = -0.58$ ) and catchment relief ( $r = -0.52$ ; Pearson's correlation coefficients).

CAIRN computes uncertainties on the catchmentwide erosion rates that include (1) the analytical uncertainty in cosmogenic nuclide concentration, (2) an uncertainty of 8.7 % on the reference production rates and (3) the uncertainty in muon production. This uncertainty estimation corresponds to the "external uncertainty" of the online calculator (Balco et al. 2008) and results in 18 to 26 % uncertainty on the catchmentwide erosion rates reported by Reber et al. (2017). The riversand calculator only takes into account the analytical uncertainty in the nuclide concentration (corresponding to the "internal uncertainty" of the online calculator), resulting in uncertainties of 3 to 5 % on the recalculated erosion rates (Supplementary Table S2).

In Figure 5c we compare erosion rates approximated from the catchment mean elevations to the riversand-calculated values, which take into account the complete production model; the approximations underestimate the latter values by 10 to 25 % for all scaling methods. The ratios of approximated to complete-production results are weakly correlated with catchment area ( $r = 0.44$ ) and mean elevation ( $r = 0.47$ ) and uncorrelated with catchment relief ( $r = 0.12$ ; all values for LSDn scaling).

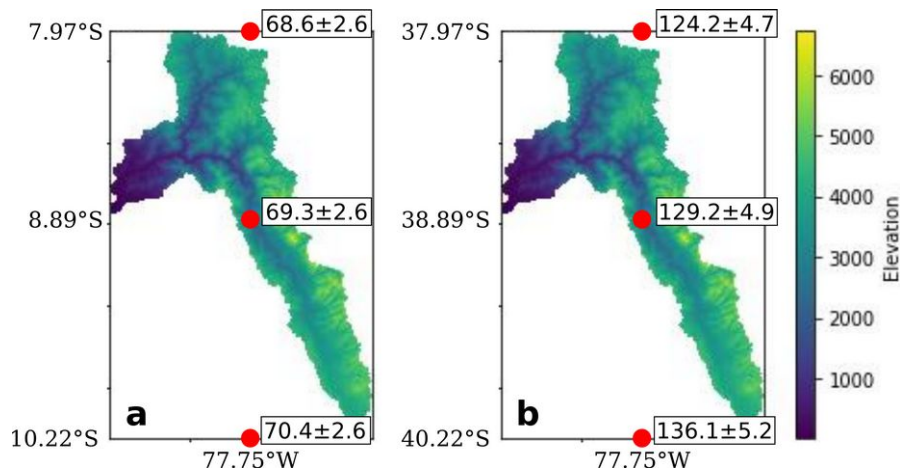


**Figure 6:** A simple test of latitudinal variation on predicted catchmentwide erosion rates using the PRCME-27 catchment of Reber et al. (2017). (a) True location of the catchment, (b) catchment shifted 30° to the south to explore a medium-latitude setting. Red points and numbers show catchmentwide erosion rates (mm/kyr, LSDn scaling) calculated for three latitudes: The middle point is the catchment centroid, i.e. the default setting in the riversand calculator; the top and bottom points show the latitude of the northernmost and southernmost tip of the catchment and corresponding erosion rates.

The dataset of the Peruvian Andes includes a large basin (sample PRCME-27) that extends 250 km from 7.9°S to 10.2°S. As a quick test to explore the effects of latitudinal variation we calculated catchmentwide erosion rates using (1) the catchment centroid coordinates (the default setting of the riversand calculator; 8.89°S / 77.75°W), (2) the latitude of the northern tip (7.97°S), and (3) the latitude of the southern tip (10.22°S; Fig. 6a). The resulting LSDn erosion rates are centroid: 69.3±2.6 mm/kyr; north: 68.6±2.6 mm/kyr; south: 70.4±2.6 mm/kyr; the differences (extreme values relative to centroid latitude) are <1.5 % in this example. The effects of latitudinal



variation on production rates are most pronounced in medium latitudes ( $\sim 20^\circ$  to  $\sim 40^\circ$ ; Lal 1991). Therefore we virtually shifted the catchment PRCME-27  $30^\circ$  to the south from its true location  $7.9$  to  $10.2^\circ\text{S}$  to a hypothetical location  $37.9$  to  $40.2^\circ\text{S}$  while keeping everything else equal (Fig. 6b). The calculated erosion rates for the shifted catchment are centroid ( $38.89^\circ\text{S}$ ):  $129.2 \pm 4.9$  mm/kyr; north ( $37.97^\circ\text{S}$ ):  $124.2 \pm 4.7$  mm/kyr; south ( $40.22^\circ\text{S}$ ):  $136.1 \pm 5.2$  mm/kyr, i.e. the results for the extreme latitudes are up to 5 % different from the centroid-based estimate. The true effects of latitudinal variation on calculated erosion rates are, of course, smaller than suggested by this appraisal. We estimate that in settings where elevation varies systematically with latitude—in particular, in large ( $>2^\circ$  latitude) medium latitude catchments that drain northward in the southern hemisphere or southward in the northern hemisphere—the inaccuracy of the presented algorithm may amount up to several percent, and a pixel based approach might provide a better estimate of the catchmentwide erosion rate.

## Discussion

Previously published pixel-based approaches to catchmentwide erosion rate calculation (Mudd et al. 2016; Charreau et al. 2019) achieve computational efficiency by using time-constant scaling methods, which do not take into account geomagnetic field fluctuations, based on the assertion that the differences between time-constant and time-dependent scaling are generally small. In two examples from the western Alps ( $\sim 45^\circ\text{N}$ ; Serra et al. 2022) and the Peruvian Andes ( $2^\circ\text{S}$  to  $20^\circ\text{S}$ ; Reber et al. 2017) we show that erosion rates calculated with the St, Lm and LSDn scaling methods differ systematically by 5 % to 20 % (Fig. 5a,b). In the latter example, the differences between time-constant and time-dependent scaling correlate with the erosion rate (Fig. 5b) suggesting that the choice of a scaling method may result in a significant bias in the geological interpretation of the results.

Balco (2020) explored the effects of time-dependent (Lm, LSDn) vs. time-constant (St) scaling on calculated erosion rates by recalculating  $>3000$  fluvial sediment datasets from the OCTOPUS database (Codilean et al. 2018). The differences between time-dependent and time-constant methods vary systematically with erosion rate: for rates  $<100$  mm/kyr the time-dependent results are up to 40 % higher, for rates  $>100$  mm/kyr time-dependent results are up to 30 % lower than time-constant results (Fig. 7). This means that ignoring geomagnetic field strength variations underestimates erosion rates in slowly eroding settings and overestimates rates in rapidly eroding settings. The trend is most pronounced at low latitudes ( $0$ - $20^\circ$ ); at latitudes  $\geq 40^\circ$  time-dependent erosion rate estimates are  $\sim 0$ - $10$  % higher than time-constant results both in slowly and rapidly eroding settings. Although these calculations are based on catchment mean elevations instead of complete production rate models the results are in excellent agreement with our findings: For the example from the Western Alps ( $300$ - $1500$  mm/kyr,  $\sim 45^\circ\text{N}$ ) Balco (2020) predicts slightly higher results for LSDn than Lm scaling ( $<10$  %); our riversand calculations yield  $5$ - $10$  % higher values for LSDn compared to Lm (Fig. 5a). For the example from the Peruvian Andes ( $10$ - $200$  mm/kyr,  $6$ - $20^\circ\text{S}$ ) Balco (2020) predicts that St scaling underestimates erosion by up to 20 % for the slowly eroding catchments and overestimates erosion by up to 10 % for the rapidly eroding catchments, a similar trend to what our riversand calculations show (Fig. 5b).

The differences between time-constant and time-dependent erosion rate estimates and, in particular, their dependence on erosion rate can be explained in terms of the integration time of erosion  $T_{\text{avg}} = z^*/E$  (where the absorption length  $z^* = 60$  cm for an attenuation length of  $160$  g/cm<sup>2</sup> and a rock density of  $2.7$  g/cm<sup>3</sup>, e.g. Dunai 2010). An erosion rate of  $100$  mm/kyr corresponds to  $T_{\text{avg}} = 6$  kyr, i.e., rapidly eroding settings ( $\sim 1000$  mm/kyr) integrate nuclide production over hundreds of years whereas slowly eroding settings ( $\sim 10$  mm/kyr) integrate production over tens of thousands of years. Because the present magnetic field seems to be anomalously strong compared to the last few million years, samples from high-erosion settings have, on average, experienced higher

magnetic field strengths and therefore lower production rates (Balco 2020). Correcting for the effects of geomagnetic field strength variations (Lm, LSDn) therefore yields lower erosion-rate estimates in rapidly eroding settings and vice versa in slowly eroding settings.

Our hypsometry-based algorithm provides a fast and efficient means to calculate catchmentwide erosion rates. The comparison with two case studies shows that (1) our calculator reproduces the results of the pixel-based approaches within a few percent if a similar scaling method is selected and (2) the results obtained with different scaling methods vary significantly (up to 20 %). A simple approximation to catchmentwide erosion rates based on the catchment mean elevation can yield meaningful results, especially when dealing with large datasets (e.g. Balco 2020), but the results may differ tens of percent from estimates that are based on a complete production rate model. Our algorithm currently does not take into account the latitudinal range of a catchment, and the calculator must be used with care when computing large ( $>2^\circ$ ) catchments at medium latitudes.

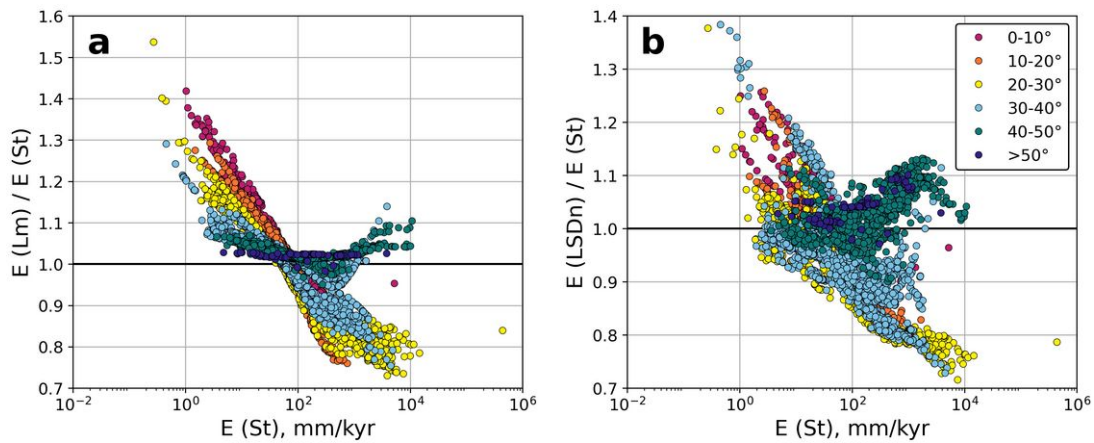


**Figure 7:** Comparison of time-dependent (a: Lm; b: LSDn) to time-constant (St) scaling for 4027 fluvial sediment datapoints from the OCTOPUS database (Codilean et al. 2018) recalculated with the online erosion rate calculator. Calculations are based on catchment centroid coordinates and mean elevation. Data points are coloured by latitude. The differences between time-dependent and time-constant methods vary systematically with erosion rate. Ignoring geomagnetic field strength variations underestimates erosion rates in slowly eroding settings and overestimates rates in rapidly eroding settings, the effect is most pronounced at low latitudes. See original analysis by Balco (2020).

## Conclusions

We present a new tool to calculate catchmentwide erosion rates from in situ  $^{10}\text{Be}$  (or  $^{26}\text{Al}$ ) cosmogenic nuclide concentrations in alluvial sediments. The riversand calculator is distributed as a platform-independent, open-source python package. The processing of geospatial data (e.g. digital elevation model, topographic shielding data, catchment outline) is performed by the calculator. Production rate calculations are performed by the online exposure age and erosion rate calculator (Balco et al. 2008), which is currently hosted on three servers (<http://hess.ess.washington.edu>, <http://stoneage.ice-d.org>, and <http://stoneage.hzdr.de>); by default, riversand sends its requests to <http://stoneage.hzdr.de>. This architecture guarantees that the results are based on the same production rates that are used by the online calculator to compute exposure ages and point-based erosion rates. Any future updates to the nuclide production scaling of the online calculator are immediately effective for the catchmentwide erosion rate calculation. Scaling methods used by the riversand calculator are those that are available from the online calculator (currently St, time-

constant Lal/Stone; Lm, time-dependent Lal/Stone; LSDn, time-dependent and nuclide-specific Lifton/Sato/Dunai methods). In contrast to existing pixel-based approaches (Mudd et al. 2016; Charreau et al. 2019) the computation time is identical for all scaling schemes, and the size and resolution of the catchment elevation model have little impact on the performance. Shielding by topography, vegetation or snow and ice can be set to a catchmentwide constant value or is derived from a raster dataset with the same projection and resolution as the elevation model. Heterogeneous quartz content in host rocks can be corrected for by a binary classification into "quartz-bearing" and "quartz-free" lithologies. The uncertainties on calculated erosion rates reflect only the analytical uncertainty on the measured nuclide concentration and correspond roughly to the "internal" uncertainties of the online calculator. A more realistic uncertainty estimate includes the uncertainties in production rates, uncertainties in shielding correction (topographic shielding and surface coverage) and the bias induced by non-uniform quartz distribution.

In two case studies, we show that erosion rates calculated with riversand agree with the results of pixel-based approaches within a few percent if based on the same scaling method. Scaling methods that do not account for geomagnetic field variations may overpredict or underpredict erosion rates by >20 %, especially for rapidly ( $\geq 1000$  mm/kyr) or slowly ( $\leq 10$  mm/kyr) eroding settings at low latitudes (Balco 2020). Therefore, the time-dependent, nuclide-specific LSDn scaling method (Lifton et al. 2014) should be the preferred scaling method for catchmentwide erosion rate calculations. Uncertainties returned by the riversand calculator reflect the analytical uncertainty in cosmogenic nuclide measurements ("internal uncertainty"). The package including documentation are available from <https://pypi.org/project/riversand/>.

## Acknowledgements

We acknowledge funding by the German Science Foundation (DFG grant STU 525/2-2 awarded to KS). This work greatly benefitted from instructive discussions at the Radiocarbon-24 conference in Zürich and with the AMS group at Helmholtz-Zentrum Dresden-Rossendorf. We thank Christopher T. Halsted for his careful review of the manuscript and Timothy Jull and Kimberley T. Elliott for editorial handling.

## References

- Balco G. 2017. Production rate calculations for cosmic-ray-muon-produced  $^{10}\text{Be}$  and  $^{26}\text{Al}$  benchmarked against geological calibration data. *Quaternary Geochronology* 39: 150–173.
- Balco G. 2020. Version 3 erosion rate calculator benchmarked, finally [WWW document]. URL: <<https://cosmognosis.wordpress.com/2020/10/10/version-3-erosion-rate-calculator-benchmarked-finally/>>.
- Belmont P, Pazzaglia FJ, Gosse JC. 2007. Cosmogenic  $^{10}\text{Be}$  as a tracer for hillslope and channel sediment dynamics in the Clearwater River, western Washington State. *Earth and Planetary Science Letters* 264(1-2): 123–135. <https://doi.org/10.1016/j.epsl.2007.09.013>
- Bierman P, Steig EJ. 1996. Estimating rates of denudation using cosmogenic isotope abundances in sediment. *Earth Surface Processes and Landforms* 21: 125–139. [https://doi.org/10.1002/\(SICI\)1096-9837\(199602\)21:2<125::AID-ESP511>3.0.CO;2-8](https://doi.org/10.1002/(SICI)1096-9837(199602)21:2<125::AID-ESP511>3.0.CO;2-8)
- Borchers B, Marrero S, Balco G, Caffee M, Goehring B, Lifton N, Nishiizumi K, Phillips F, Schaefer J, Stone J. 2016. Geological calibration of spallation production rates in the CRONUS-Earth project. *Quaternary Geochronology* 31: 188–198. <https://doi.org/10.1016/j.quageo.2015.01.009>
- Braucher R, Merchel S, Borgomano J, Bourlès DL. 2011. Production of cosmogenic radionuclides at great depth: A multi element approach. *Earth and Planetary Science Letters* 309(1-2): 1–9.

- Brown ET, Stallard RF, Larsen MC, Raisbeck GM, Yiou F. 1995. Denudation rates determined from the accumulation of in situ-produced  $^{10}\text{Be}$  in the Luquillo Experimental Forest, Puerto Rico. *Earth and Planetary Science Letters* 129: 193–202. [https://doi.org/10.1016/0012-821X\(94\)00249-X](https://doi.org/10.1016/0012-821X(94)00249-X)
- Carretier S, Regard V, Vassallo R, Martinod J, Christophoul F, Gayer E, Audin L, Lagane C. 2015. A note on  $^{10}\text{Be}$ -derived mean erosion rates in catchments with heterogeneous lithology: Examples from the western Central Andes. *Earth Surface Processes and Landforms* 40(13): 17191–1729. <https://doi.org/10.1002/esp.3748>
- Charreau J, Blard PH, Zumaque J, Martin LCP, Delobel T, Szafran L. 2019. Basinga: A cell-by-cell GIS toolbox for computing basin average scaling factors, cosmogenic production rates and denudation rates. *Earth Surface Processes and Landforms* 44: 2349–2365. <https://doi.org/10.1002/esp.4649>
- Codilean AT. 2006. Calculation of the cosmogenic nuclide production topographic shielding scaling factor for large areas using DEMs. *Earth Surface Processes and Landforms* 31: 785–794. <https://doi.org/10.1002/esp.1336>
- Codilean AT, Munack H, Cohen TJ, Saktura WM, Gray A, Mudd SM. 2018. OCTOPUS: an open cosmogenic isotope and luminescence database. *Earth System Science Data* 10: 2123–2139. <https://doi.org/10.5194/essd-10-2123-2018>
- Compo GP, Whitaker JS, Sardeshmukh PD, Matsui N, Allan RJ, Yin X, Gleason BE, Vose RS, Rutledge G, Bessemoulin P, Brönnimann S, Brunet M, Crouthamel RI, Grant AN, Groisman PY, Jones PD, Kruk MC, Kruger AC, Marshall GJ, Maugeri M, Mok HY, Nordli Ø, Ross TF, Trigo RM, Wang XL, Woodruff SD, Worley SJ. 2011. The Twentieth Century Reanalysis Project. *Quaternary Journal of the Royal Meteorological Society* 137: 1–28. <https://doi.org/10.1002/qj.776>
- Delunel R, Van Der Beek PA, Carcaillet J, Bourlès DL, Valla PG. 2010. Frost-cracking control on catchment denudation rates: Insights from in situ produced  $^{10}\text{Be}$  concentrations in stream sediments (Ecrins–Pelvoux massif, French Western Alps). *Earth and Planetary Science Letters* 293(1–2): 72–83. <https://doi.org/10.1016/j.epsl.2010.02.020>
- Desilets D, Zreda MG, Prabu T. 2006. Extended scaling factors for in situ cosmogenic nuclides: New measurements at low latitude. *Earth and Planetary Science Letters* 246: 265–276.
- Dunai TJ. 2001. Influence of secular variation of the geomagnetic field on production rates of in situ produced cosmogenic nuclides. *Earth and Planetary Science Letters* 193: 197–212.
- Dunai TJ. 2010. *Cosmogenic nuclides: Principles, concepts and applications in the Earth surface sciences*. Cambridge University Press.
- Godard V, Bourlès DL, Spinabella F, Burbank DW, Bookhagen B, Fisher GB, Moulin A, Léanni L. 2014. Dominance of tectonics over climate in Himalayan denudation. *Geology* 42(3): 243–246. <https://doi.org/10.1130/G35342.1>
- Granger DE, Kirchner JW, Finkel R. 1996. Spatially averaged long-term erosion rates measured from in situ-produced cosmogenic nuclides in alluvial sediment. *The Journal of Geology* 104: 249–257. <https://doi.org/10.1086/629823>
- Jarvis A, Reuter HI, Nelson A, Guevara E. 2008. Hole-filled SRTM for the globe Version 4. Retrieved from <http://srtm.csi.cgiar.org> (CGIAR-CSI SRTM 90 m Database).
- Lal D. 1991. Cosmic ray labeling of erosion surfaces: in situ nuclide production rates and erosion models. *Earth and Planetary Science Letters* 104: 424–43. [https://doi.org/10.1016/0012-821X\(91\)90220-C](https://doi.org/10.1016/0012-821X(91)90220-C)
- Lifton N, Smart DF, Shea MA. 2008. Scaling time-integrated in situ cosmogenic nuclide production rates using a continuous geomagnetic model. *Earth and Planetary Science Letters* 268: 190–201.
- Lifton N, Sato T, Dunai TJ. 2014. Scaling in situ cosmogenic nuclide production rates using analytical approximations to atmospheric cosmic-ray fluxes. *Earth and Planetary Science Letters* 386: 149–160.
- Lifton N. 2016. Implications of two Holocene time-dependent geomagnetic models for cosmogenic nuclide production rate scaling. *Earth and Planetary Science Letters* 433: 257–268.
- Lupker M, Blard PH, Lavé J, France-Lanord C, Leanni L, Puchol N, Charreau J, Bourlès D. 2012.  $^{10}\text{Be}$ -derived Himalayan denudation rates and sediment budgets in the Ganga basin. *Earth and Planetary Science Letters* 333: 146–156.
- Marrero SM, Phillips FM, Borchers B, Lifton N, Aumer R, Balco G. 2016. Cosmogenic nuclide systematics and the CRONUScal program. *Quaternary Geochronology* 31: 160–187.
- Martin LCP, Blard PH, Balco G, Lavé J, Delunel R, Lifton N, Laurent V. 2017. The CREp program and the ICE-D production rate calibration database: A fully parameterizable and updated online tool to compute cosmic-ray exposure ages. *Quaternary Geochronology* 38: 25–49. <https://doi.org/10.1016/J.QUAGEO.2016.11.006>
- Muscheler R, Beer J, Kubik PW, Synal HA. 2005. Geomagnetic field intensity during the last 60,000 years based on  $^{10}\text{Be}$  and  $^{36}\text{Cl}$  from the Summit ice cores and 14C. *Quaternary Science Reviews* 24: 1849–1860. <https://doi.org/10.1016/j.quascirev.2005.01.012>

- Mudd SM, Harel MA, Hurst MD, Grieve SWD, Marrero SM. 2016. The CAIRN method: automated, reproducible calculation of catchment-averaged denudation rates from cosmogenic nuclide concentrations. *Earth Surface Dynamics* 4: 655–674. <https://doi.org/10.5194/esurf-4-655-2016>
- NASA JPL. 2021. *NASADEM Merged DEM Global 1 arc second V001*. Distributed by OpenTopography. <https://doi.org/10.5069/G93T9FD9>. Accessed: 2022-11-29
- Nishiizumi K, Winterer EL, Kohl CP, Klein J, Middleton R, Lal D, Arnold JR. 1989. Cosmic ray production rates of  $^{10}\text{Be}$  and  $^{26}\text{Al}$  in quartz from glacially polished rocks. *Journal of Geophysical Research: Solid Earth* 94(B12): 17907–17915.
- Portenga EW, Bierman PR. 2011. Understanding Earth's eroding surface with  $^{10}\text{Be}$ . *GSA Today* 21(8): 4–10. <https://doi.org/10.1130/G111A.1>
- Radok U, Allison I, Wendler G. 1996. Atmospheric surface pressure over the interior of Antarctica. *Antarctic Science* 8: 209–217.
- Reber R, Delunel R, Schlunegger F, Litty C, Madella A, Akçar N, Christl M. 2017. Environmental controls on  $^{10}\text{Be}$ -based catchment-averaged denudation rates along the western margin of the Peruvian Andes. *Terra Nova* 29(5): 282–293.
- Safran EB, Bierman PR, Aalto R, Dunne T, Whipple KX, Caffee M. 2005. Erosion rates driven by channel network incision in the Bolivian Andes. *Earth Surface Processes and Landforms* 30(8): 1007–1024.
- Scherler D, Bookhagen B, Strecker MR. 2014. Tectonic control on  $^{10}\text{Be}$ -derived erosion rates in the Garhwal Himalaya, India. *Journal of Geophysical Research: Earth Surface* 119(2): 83–105.
- Schwanghart W, Scherler D. 2014. Short Communication: TopoToolbox 2 – MATLAB-based software for topographic analysis and modeling in Earth surface sciences. *Earth Surface Dynamics* 2: 1–7. <https://doi.org/10.5194/esurf-2-1-2014>
- Serra E, Valla PG, Delunel R, Gribenski N, Christl M, Akçar N. 2022. Spatio-temporal variability and controlling factors for postglacial denudation rates in the Dora Baltea catchment (western Italian Alps). *Earth Surface Dynamics* 10(3): 493–512.
- Stone JO. 2000. Air pressure and cosmogenic isotope production. *Journal of Geophysical Research: Solid Earth* 105: 23753–23759. <https://doi.org/10.1029/2000JB900181>
- Uppala SM, Kållberg PW, Simmons AJ, Andrae U, da Costa Bechtold V, Fiorino M, Gibson JK, Haseler J, Hernandez A, Kelly GA, Li X, Onogi K, Saarinen S, Sokka N, Allan RP, Andersson E, Arpe K, Balmaseda MA, Beljaars ACM, van de Berg L, Bidlot J, Bormann N, Caires S, Chevallier F, Dethof A, Dragosavac M, Fisher M, Fuentes M, Hagemann S, Hólm E, Hoskins BJ, Isaksen I, Janssen PAEM, Jenne R, McNally AP, Mahfouf JF, Morcrette JJ, Rayner NA, Saunders RW, Simon P, Sterl A, Trenberth KE, Untch A, Vasiljevic D, Viterbo P, Woollen J. 2005. The ERA-40 re-analysis. *Quarterly Journal of the Royal Meteorological Society* 131: 2961–3012. <https://doi.org/10.1256/qj.04.176>
- von Blanckenburg F. 2005. The control mechanisms of erosion and weathering at basin scale from cosmogenic nuclides in river sediment. *Earth and Planetary Science Letters* 237: 462–479. <https://doi.org/10.1016/j.epsl.2005.06.030>